The influence of heme ruffling on spin densities in ferricytochromes *c* probed by heme core ^{13}C NMR

Jesse G. Kleingardner, Sarah E. J. Bowman, Kara L. Bren*

Department of Chemistry, University of Rochester, Rochester, New York 14627-0216

Supporting Information
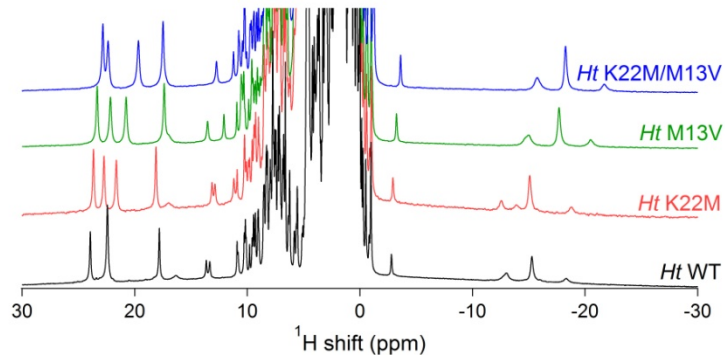
Figure S1. ^{1}H NMR spectra of the *Ht* series of variants and *Ht* WT in the Fe^{III} oxidation state.
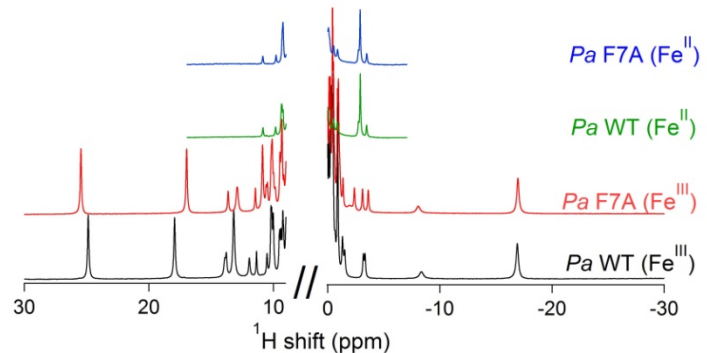

Figure S2. ^{1}H NMR spectra of *Pa* WT and *Pa* F7A in both the Fe^{III} and Fe^{II} oxidation states.
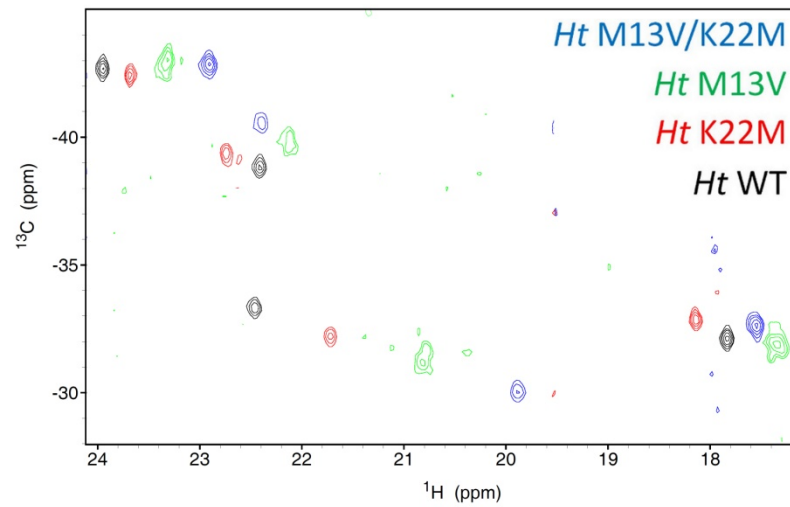
Figure S3. Overlay of natural-abundance ^{1}H-^{13}C HMQC spectra showing heme methyls of *Ht* series of mutants in the Fe^{III} oxidation state.
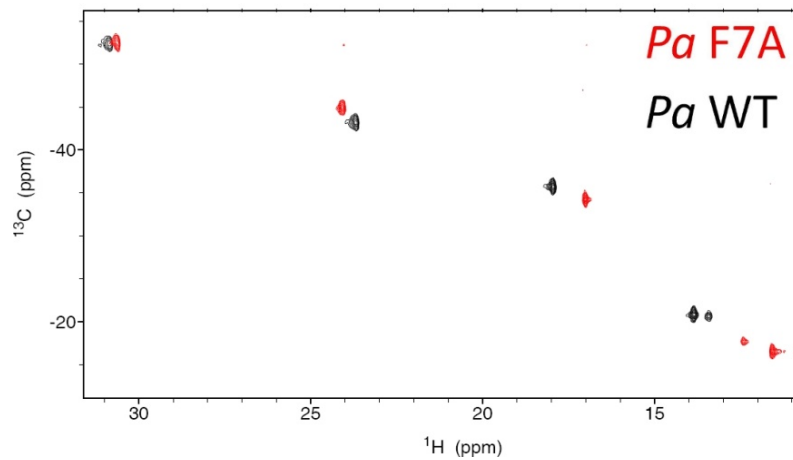
**Figure S4.** Overlay of natural-abundance ^{1}H-^{13}C HMQC spectra showing heme methyls of *Pa* WT and *Pa* F7A in the Fe^{III} oxidation state.
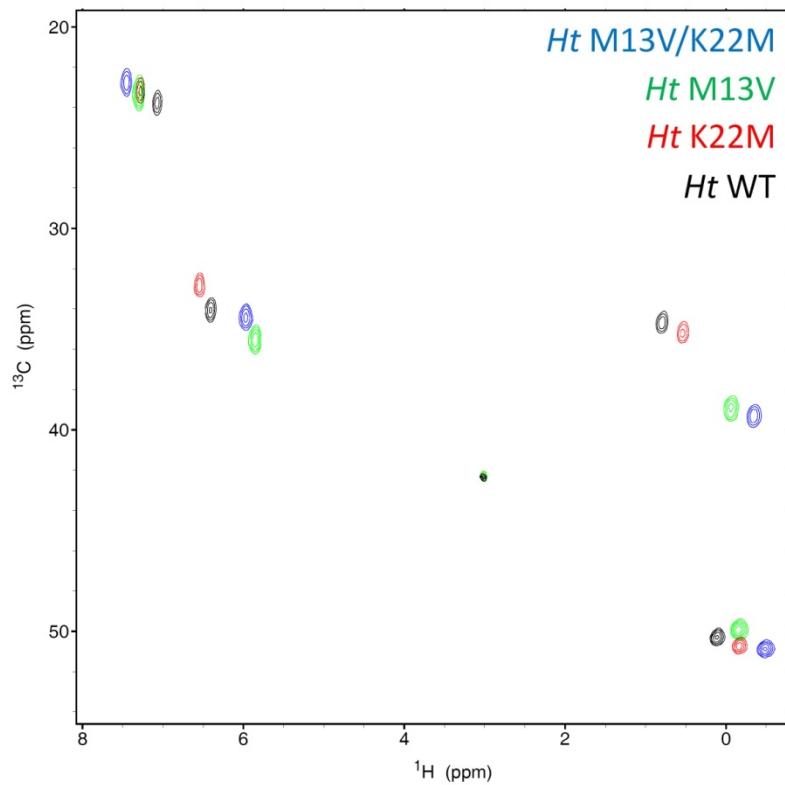
Figure S5. Overlay of ^{1}H-^{13}C HMQC spectra of 5-^{13}C-ALA labeled *Ht*-series of mutants in the Fe^{III} oxidation state.
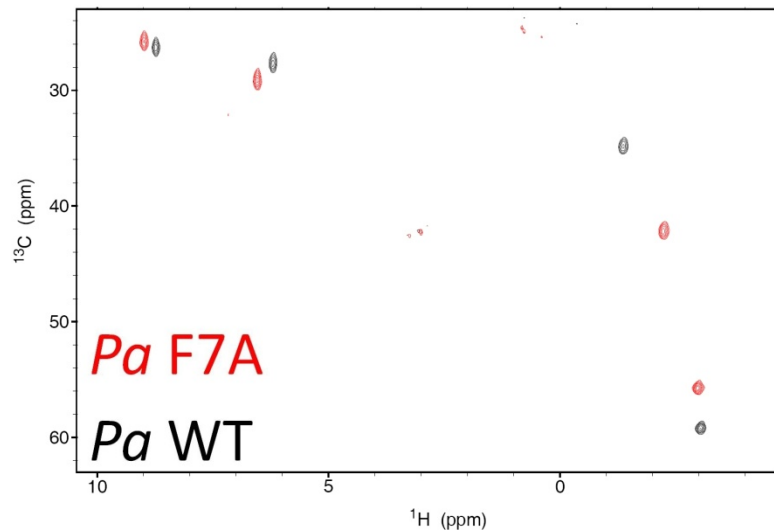
Figure S6. Overlay of ^{1}H-^{13}C HMQC spectra of 5-^{13}C-ALA-labeled *Pa* WT and *Pa* F7A in the Fe^{III} oxidation state.
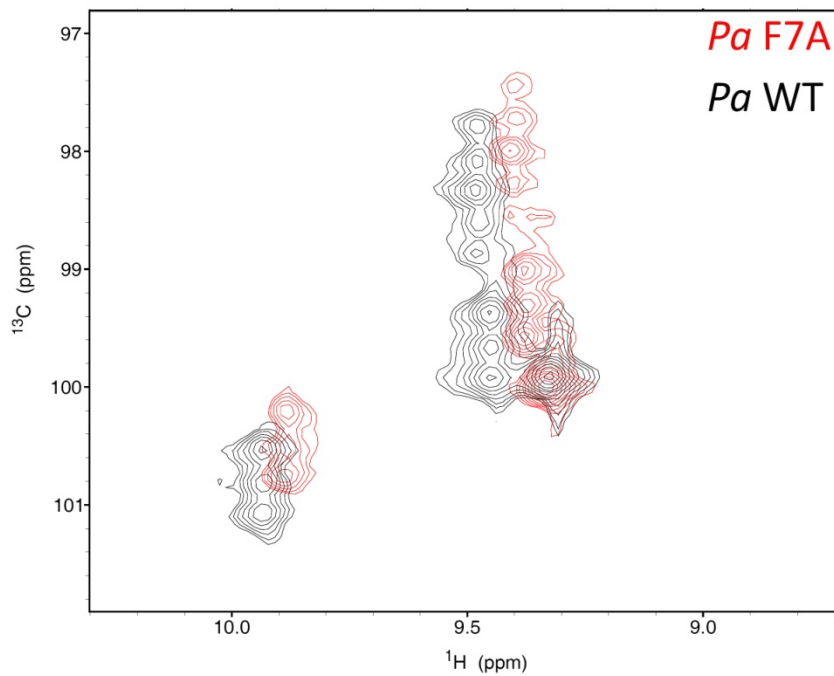
Figure S7. Overlay of ^{1}H-^{13}C HMQC spectra of 5-^{13}C-ALA labeled *Pa* WT and *Pa* F7A in the Fe^{II} oxidation state.
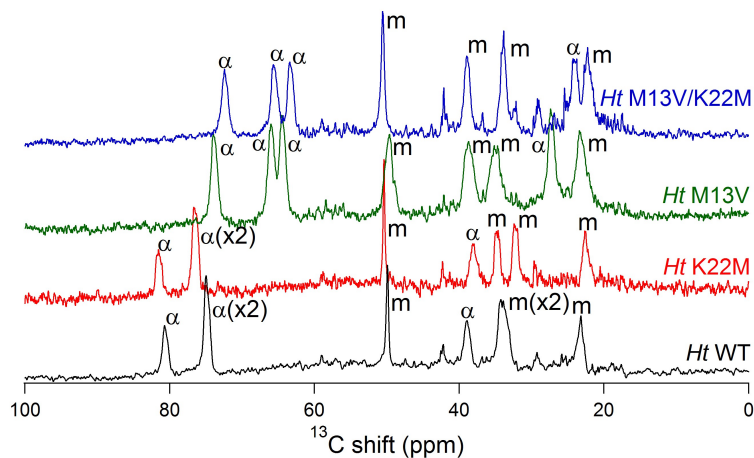
Figure S8. 1-D ^{13}C NMR spectra of the *Ht* series of variants in the Fe^{III} oxidation state labeled with 5-^{13}C-ALA. Peaks are labeled according to their assignment as a meso (m) or α-pyrrole (α) carbon.

5
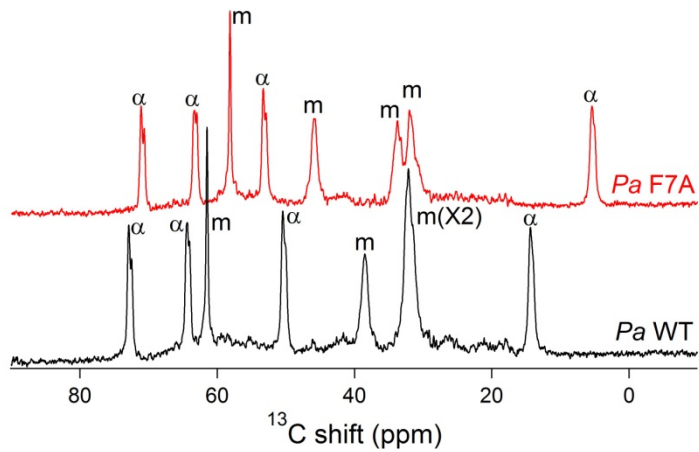
Figure S9. 1-D ^{13}C NMR spectra of *Pa* and *Pa* F7A in the Fe^{III} oxidation state labeled with 5-^{13}C-ALA.
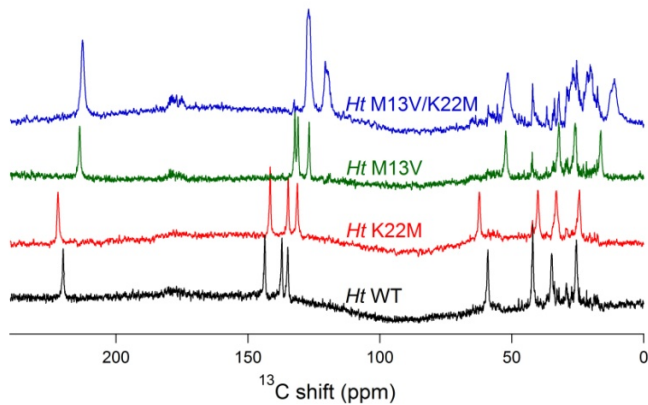
Figure S10. 1-D ^{13}C NMR spectra of the 4-^{13}C-ALA labeled samples of the *Ht* series in the Fe^{III} oxidation state.
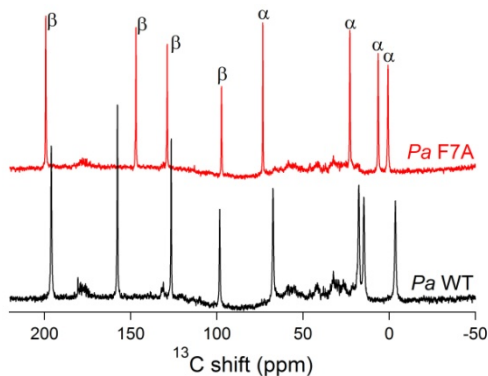
Figure S11. 1-D ^{13}C NMR spectra of the 4-^{13}C-ALA labeled samples of *Pa* WT and *Pa* F7A in the Fe^{III} oxidation state.
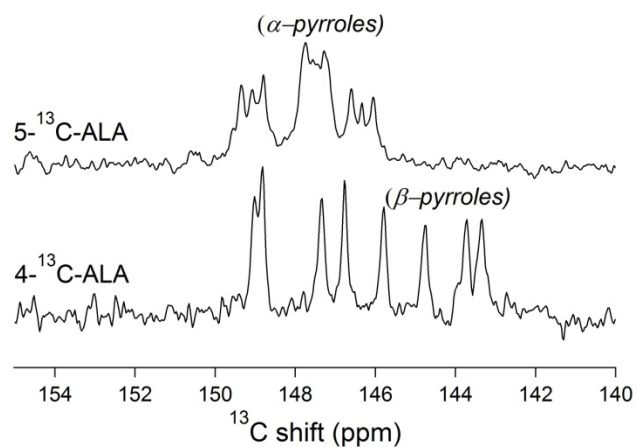
Figure S12. 1-D ^{13}C NMR spectra of *Pa* WT with both ALA labeling patterns in the Fe^{II} oxidation state. The splittings observed in the spectrum of the 5-^{13}C-ALA labeled sample are a result of adjacent ^{13}C isotopes with a $^{1}J_{CC}$ value of ~ 67 Hz. The samples are also only partially labeled, accounting for the complexity of the observed spectrum.
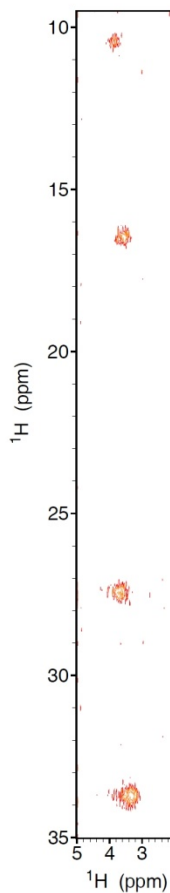
Figure S13. EXSY NMR spectrum of *Pa* F7A showing crosspeaks of the heme methyl ^{1}H resonances between the oxidized and reduced states.

7
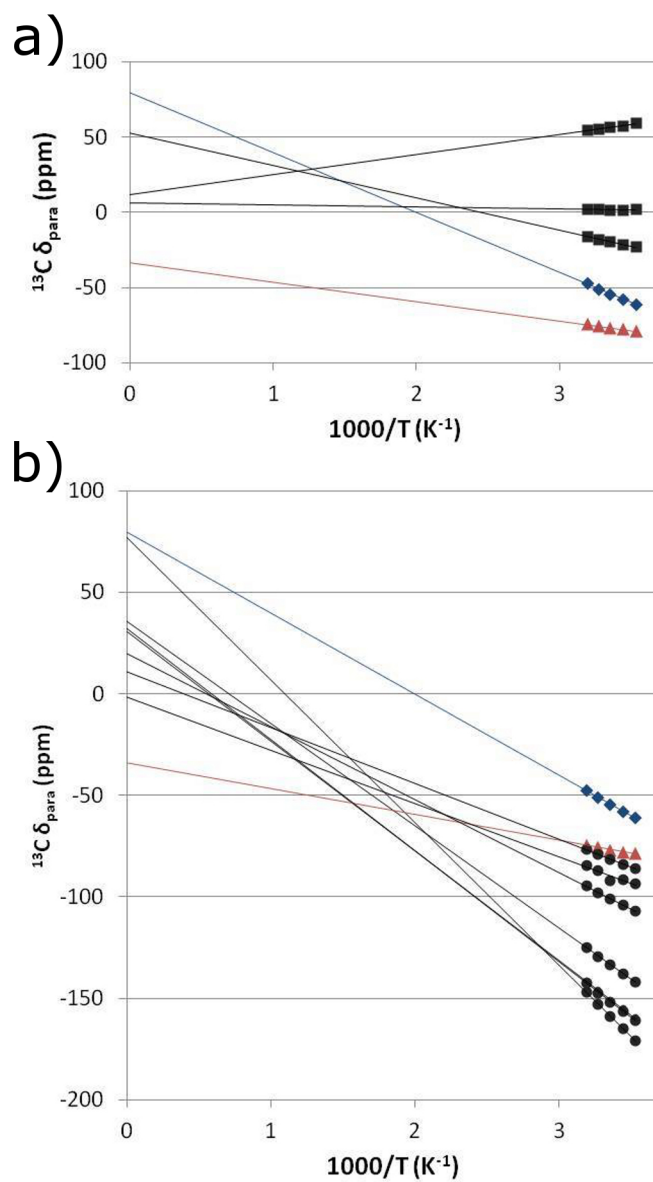
Figure S14. (a) Temperature dependence of the three unambiguously assigned β-pyrrole ^{13}C shifts of *Pa* F7A (black squares) compared to the two peaks with ambiguous assignments (blue diamonds, red triangles). (b) Temperature dependence of the seven unambiguously assigned α-pyrrole ^{13}C shifts of *Pa* F7A (black circles) compared to the two peaks with ambiguous assignments (blue diamonds, red triangles). (a and b) The blue diamonds represent the peak tentatively assigned to a β-pyrrole carbon based on its lower shift and temperature dependence. The red triangles represent the peak tentatively assigned to an α-pyrrole carbon. Individual shifts are reported in Table S11. Data for *Pa* WT is shown in Figure 3 of the main article.

8
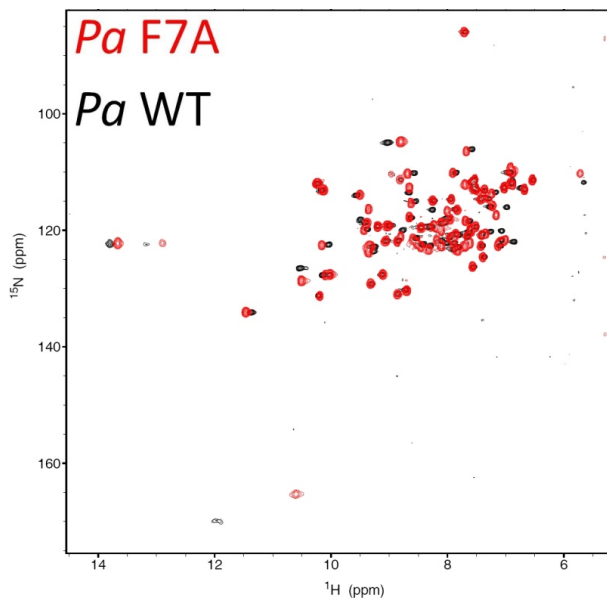
Figure S15. Overlay of ^{1}H-^{15}N HSQC spectra of Fe^{III} *Pa* WT and *Pa* F7A at 25 °C. The axial His δ$_1$-NH peaks are the two with the ^{15}N shift > 160 ppm.
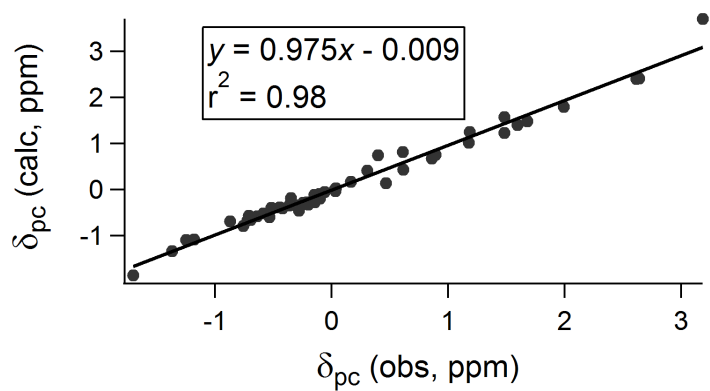
Figure S16. Plot of calculated versus observed pseudocontact shifts used for the determination of the magnetic axes of *Ht* WT at 40 °C.

Equations S1 and S2. Inclusion of a ligand-centered pseudocontact shift term in the porphyrin spin density calculations.

Equation S1:

$$\left(\delta_{FC} + \delta_{PC}^{LC}\right)_{\beta} = \left[\left(\frac{\beta g S(S+1)}{\gamma_I \hbar 3 k_B T}\right)(S^C + 3Q_{CC'}^C + Q_{C'C}^C) + D\right]\rho_{\beta}^{\pi} + \left(\frac{\beta g S(S+1)}{\gamma_I \hbar 3 k_B T}\right)(Q_{C'C}^C \rho_{\alpha}^{\pi})$$

Equation S2:

$$\left(\delta_{FC} + \delta_{PC}^{LC}\right)_{\alpha} = \left[\left(\frac{\beta g S(S+1)}{\gamma_I \hbar 3 k_B T}\right)(S^C + 2Q_{CC'}^C + Q_{CN}^C) + D\right]\rho_{\alpha}^{\pi} + \left(\frac{\beta g S(S+1)}{\gamma_I \hbar 3 k_B T}\right)(Q_{C'C}^C \rho_{\beta}^{\pi} + Q_{C'C}^C \rho_{meso}^{\pi} + Q_{NC}^C \rho_{N}^{\pi})$$

Table S1. Euler rotation angles and magnetic anisotropies Pa cyt c_{551} at 25 °C and Ht cyt c_{552} at 40 °C.

	α	β	γ	$\Delta\chi_{ax}$ (/10^{-32} m^3)	$\Delta\chi_{rh}$ (/10^{-32} m^3)
Pa WT[a]	90°	5°	258°	2.98	-1.13
Pa F7A[b]	90°	5°	258°	2.86	-1.26
Ht WT[c]	81°	-3.5°	230°	2.81	-0.494
Ht K22M[b]	81°	-3.5°	230°	2.66	-0.498
Ht M13V[b]	81°	-3.5°	230°	2.52	-0.506
Ht M13V/K22M[b]	81°	-3.5°	230°	2.44	-0.514

[a]Values taken from ref. 1. [b]Values scaled from Pa or Ht WT[1] according to the variant's g values determined from EPR.[2] [c]Values determined herein.

Table S2. Selected chemical shifts of heme and axial Met of reduced (Fe^{II}) *Pa* WT, determined herein. Shifts for the axial His of reduced *Ht* are provided (from ref. 3). These values were used as diamagnetic reference shifts.

	δ_{dia} (ppm)
^1H methyl	3.51
^{13}C methyl	14.68
^1H meso	9.55
^{13}C meso	99.7
^{13}C α-pyrrole	147.7
^{13}C β-pyrrole	144.8
Met61 ε-C^1H_3	-2.9
His16 δ_1-$^{15}N^a$	120.4
His 16 δ_1-N^1H^a	6.73

[a]These values are assignments of reduced *Ht* cyt c_{552}.[3]

Table S3. Values used for the proportionality constants between spin density and the hyperfine coupling constant, A^H. These are used in Equations 6–10 in the main text.

Q_{CH}^H	-63 MHz
$Q_{C'C}^C$	-39 MHz
S^C	-35.5 MHz
$Q_{CC'}^C$	40.3 MHz
Q_{CH}^C	54.6 MHz
Q_{CN}^C	40.3 MHz
Q_{NC}^C	-39 MHz

Table S4. [1]H resonance assignments for *Ht* WT determined at 40 °C at pH 7.0. Assignments were performed in both the ferric (ox) and ferrous (red) states. The pseudocontact shifts (δ_{pc}) were calculated by subtracting δ_{red} from δ_{ox}, and were used to determine the magnetic axes and anisotropy. QB designates methyl groups for which rotationally averaged coordinates were used in the magnetic axes fitting procedure.

Residue	Atom	δ_{ox}	δ_{red}	δ_{pc}	Residue	Atom	δ_{ox}	δ_{red}	δ_{pc}
A7	HN	7.48	7.85	-0.36	A45	HN	8.57	8.71	-0.14
K8	HN	7.95	8.08	-0.13	A45	HN	3.50	3.85	-0.35
Q9	HN	8.35	8.44	-0.10	A45	QB	1.23	1.37	-0.15
K10	HN	7.89	8.41	-0.52	I48	HN	8.51	7.90	0.62
C12	HN	8.10	8.85	-0.76	K50	HN	9.32	7.84	1.48
C12	HA	3.34	5.04	-1.70	K50	HA	5.09	3.91	1.19
M13	HN	8.36	7.89	0.47	G51	HN	10.31	7.12	3.19
M13	HN	6.25	4.65	1.60	G52	HN	10.12	7.50	2.62
D17	HN	10.20	7.56	2.64	V55	HN	9.83	10.28	-0.45
D17	HA	5.87	4.39	1.48	V55	HA	3.73	3.94	-0.21
L18	HN	9.13	8.24	0.89	V55	HB	2.06	2.59	-0.53
V23	HN	7.70	7.08	0.61	W56	HN	9.58	10.45	-0.87
V23	HA	3.65	3.99	-0.35	W56	HA	4.28	4.70	-0.42
A26	HN	9.47	8.30	1.18	W56	HD1	6.40	7.76	-1.37
A26	HA	5.81	3.82	1.99	W56	HE1	10.94	12.12	-1.18
A26	QB	1.51	0.65	0.86	V59	HN	7.00	7.72	-0.72
Y27	HN	9.45	7.77	1.68	V59	HA	3.93	4.56	-0.64
Y27	HA	4.41	4.01	0.40	V59	HB	1.03	2.28	-1.25
D29	HN	7.07	6.76	0.31	L74	HN	8.29	8.88	-0.59
V30	HN	7.76	7.59	0.17	L74	HA	3.63	4.33	-0.70
V30	HA	3.79	4.06	-0.27	I78	HN	8.00	8.71	-0.71
V30	HB	2.17	2.37	-0.20	I78	HA	2.24	2.48	-0.24
K32	HN	7.36	7.33	0.03	I81	HN	7.08	7.18	-0.10
K32	HA	4.07	4.13	-0.06	I81	HA	3.68	3.65	0.03
L44	HN	8.54	8.77	-0.23	I81	HB	1.67	1.63	0.04
L44	HA	3.29	3.57	-0.28					

Table S5. Contributions to the paramagnetic chemical shifts (ppm) of the heme and axial ligands of *Ht* WT and *Ht* K22M at 40 °C.

	Ht WT			*Ht* K22M		
	δ_{para}	δ_{PC}^{MC}	$\delta_{FC} + \delta_{PC}^{LC}$	δ_{para}	δ_{PC}^{MC}	$\delta_{FC} + \delta_{PC}^{LC}$
^{1}H methyl	18.15	–2.61	20.76	18.02	–2.48	20.50
^{13}C methyl	–51.4	–4.3	–47.1	–51.4	–4.1	–47.3
^{1}H meso	–5.92	–7.71	1.79	–5.97	–7.29	1.32
^{13}C meso	–64.0	–17.9	–46.0	–64.2	–17.0	–47.2
^{13}C α-pyrrole	–93.9	–23.6	–70.2	–93.6	–22.3	–71.2
^{13}C β-pyrrole	14.1	–9.2	23.3	12.6	–8.7	21.3

Table S6. Contributions to the paramagnetic chemical shifts (ppm) of the heme and axial ligands of *Ht* M13V and *Ht* M13V/K22M at 40 °C.

	Ht M13V			*Ht* M13V/K22M		
	δ_{para}	δ_{PC}^{MC}	$\delta_{FC} + \delta_{PC}^{LC}$	δ_{para}	δ_{PC}^{MC}	$\delta_{FC} + \delta_{PC}^{LC}$
^{1}H methyl	17.39	–2.36	19.76	17.07	–2.30	19.37
^{13}C methyl	–51.1	–3.9	–47.2	–51.2	–3.8	–47.4
^{1}H meso	–6.28	–6.90	0.62	–6.37	–6.67	0.30
^{13}C meso	–62.8	–16.1	–46.7	–62.8	–15.5	–47.3
^{13}C α-pyrrole	–102.9	–21.1	–81.8	–105.8	–20.4	–85.4
^{13}C β-pyrrole	6.2	–8.2	14.4	1.9	–7.9	9.8

Table S7. Contributions to the sum of the average contact and ligand-centered pseudocontact shifts (in ppm) for selected heme nuclei. The contributions from the spin density on each of the nuclei are shown independently. The data shown are for *Ht* WT at 40 °C.

	ρ_{meso}^{π}	$\rho_{\beta-pyrrole}^{\pi}$	$\rho_{\alpha-pyrrole}^{\pi}$	$\rho_{N-pyrrole}^{\pi}$
^{1}H meso	1.8	-	-	-
^{13}C methyl	-	–47.1	-	-
^{13}C meso	–9.9	-	–36.2	-
^{13}C β-pyrrole	-	41.4	–18.1	-
^{13}C α-pyrrole	4.4	–47.1	34.0	–61.4

Table S8. Contributions to the change in the average contact and ligand-centered pseudocontact shifts (in ppm) for selected heme nuclei. The contributions from the spin density on each of the nuclei are shown independently. The data shown are for *Ht* K22M−WT at 40 °C.

	ρ^π_{meso}	$\rho^\pi_{\beta-pyrrole}$	$\rho^\pi_{\alpha-pyrrole}$	$\rho^\pi_{N-pyrrole}$
^{1}H meso	−0.55	-	-	-
^{13}C methyl	-	−0.16	-	-
^{13}C meso	3.04	-	−4.24	-
^{13}C β-pyrrole	-	0.14	−2.12	-
^{13}C α-pyrrole	−1.35	−0.16	3.98	−3.48

Table S9. Contributions to the change in the average contact and ligand-centered pseudocontact shifts (in ppm) for selected heme nuclei. The contributions from the spin density on each of the nuclei are shown independently. The data shown are for *Ht* M13V−WT at 40 °C.

	ρ^π_{meso}	$\rho^\pi_{\beta-pyrrole}$	$\rho^\pi_{\alpha-pyrrole}$	$\rho^\pi_{N-pyrrole}$
^{1}H meso	−2.73	-	-	-
^{13}C methyl	-	0.40	-	-
^{13}C meso	15.1	-	−16.1	-
^{13}C β-pyrrole	-	−0.35	−8.03	-
^{13}C α-pyrrole	−6.73	0.40	15.1	−20.3

Table S10. Contributions to the change in the average contact and ligand-centered pseudocontact shifts (in ppm) for selected heme nuclei. The contributions from the spin density on each of the nuclei are shown independently. The data shown are for *Ht* M13V/K22M−WT at 40 °C.

	ρ^π_{meso}	$\rho^\pi_{\beta-pyrrole}$	$\rho^\pi_{\alpha-pyrrole}$	$\rho^\pi_{N-pyrrole}$
^{1}H meso	−4.07	-	-	-
^{13}C methyl	-	0.53	-	-
^{13}C meso	22.5	-	−24.3	-
^{13}C β-pyrrole	-	−0.46	−12.1	-
^{13}C α-pyrrole	−10.0	0.53	22.8	−28.5

Table S11. Temperature dependent shifts of meso, α-pyrrole, and β-pyrrole core heme ^{13}C shifts in ppm collected for Fe[III] *Pa* WT at 25 °C.

[13]C labeling pattern	Nucleus	283 K	290.5 K	298 K	305.5 K	313 K
5-^{13}C-ALA	meso	19.5	22.9	26.1	29.4	32.0
	meso	22.7	25.2	27.3	29.4	32.0
	meso	30.6	32.6	34.5	36.6	38.5
	meso	56.3	56.8	59.0	60.3	61.5
5-^{13}C-ALA	α-pyrrole	-5.7	-0.7	4.0	9.2	14.3
	α-pyrrole	37.9	40.6	43.5	46.8	50.3
	α-pyrrole	54.7	57.7	59.0	61.6	64.3
	α-pyrrole	62.8	65.0	67.4	69.9	72.8
4-^{13}C-ALA	α-pyrrole	-27.8	-21.8	-16.0	-9.9	-3.6
	α-pyrrole	-4.2	0.5	5.0	9.8	14.7
	α-pyrrole	-0.1	4.2	8.4	12.9	17.7
	α-pyrrole	61.7	62.7	63.9	65.5	67.4
4-^{13}C-ALA	β-pyrrole	84.1	87.5	90.9	94.5	98.3
	β-pyrrole	117.3	119.3	121.5	123.8	126.5
	β-pyrrole	155.8	156.1	156.4	156.9	157.6
	β-pyrrole	201.1	199.3	197.9	196.8	196.0

Table S12. Temperature dependent shifts of meso, α-pyrrole, and β-pyrrole core heme ^{13}C shifts in ppm collected for Fe[III] *Pa* F7A at 25 °C.

[13]C labeling pattern	Nucleus	283 K	290.5 K	298 K	305.5 K	313 K
5-^{13}C-ALA	meso	19.2	22.3	25.4	28.8	31.8
	meso	23.9	26.4	28.8	31.3	33.8
	meso	37.5	39.9	41.9	43.9	45.8
	meso	52.8	54.2	58.3	56.9	58.1
5-^{13}C-ALA	α-pyrrole	-13.3	-8.8	-4.4	0.5	5.3
	α-pyrrole	40.9	43.8	46.7	49.9	53.2
	α-pyrrole	54.2	56.3	55.6	60.7	63.2
	α-pyrrole	61.6	63.8	66.0	68.4	71.0
4-^{13}C-ALA	α-pyrrole	-23.1	-17.1	-11.4	-5.3	0.7
	α-pyrrole	-11.9	-7.5	-3.2	1.6	6.4
	α-pyrrole	5.7	10.0	14.1	18.5	22.8
	α-pyrrole	68.9	69.8	70.7	72.0	73.3
4-^{13}C-ALA	β-pyrrole	83.7	86.9	90.2	93.6	97.3
	β-pyrrole	121.5	123.1	124.8	126.7	128.8
	β-pyrrole	146.4	146.2	146.1	146.4	146.9
	β-pyrrole	203.7	202.2	201.0	200.0	199.2

Table S13. List of heme ^{1}H and ^{13}C shifts in ppm used in this study. Data for the Fe^{III} forms of *Pa* cyt c_{551} and *Ht* cyt c_{552} variants were collected at 25 °C and 40 °C, respectively. Specific assignments were not made.

Nucleus	*Pa* WT	*Pa* F7A	*Ht* WT	*Ht* K22M	*Ht* M13V	*Ht* M13V /K22M
^{13}C meso[a]	26.3	25.8	23.8	23.2	23.3	22.8
^{13}C meso[a]	27.7	29.1	34.1	32.9	35.5	34.5
^{13}C meso[a]	34.8	42.2	34.7	35.2	38.9	39.3
^{13}C meso[a]	59.2	55.7	50.3	50.7	49.9	50.9
^{1}H meso[a]	8.73	8.99	0.14	-0.14	-0.12	-0.45
^{1}H meso[a]	6.20	6.54	0.83	0.57	-0.03	-0.32
^{1}H meso[a]	-1.36	-2.23	6.44	6.58	5.88	6.00
^{1}H meso[a]	-3.03	-2.97	7.10	7.31	7.33	7.48
^{13}C α-pyrrole[a]	4.0	-4.4	38.9	38.2	27.3	24.1
^{13}C α-pyrrole[a]	43.5	46.7	74.9	76.6	64.4	63.3
^{13}C α-pyrrole[a]	59.0	55.6	74.9	76.6	66.0	65.6
^{13}C α-pyrrole[a]	67.4	66.0	80.6	81.6	73.9	72.4
^{13}C α-pyrrole[b]	-16.0	-11.4	25.5	24.5	16.4	11.3
^{13}C α-pyrrole[b]	5.0	-3.2	34.9	33.2	26.0	20.3
^{13}C α-pyrrole[b]	8.4	14.1	42.1	40.1	32.2	26.6
^{13}C α-pyrrole[b]	63.9	70.7	59.1	62.3	52.3	51.7
^{13}C β-pyrrole[b]	90.9	90.2	134.9	131.3	126.9	120.1
^{13}C β-pyrrole[b]	121.5	124.8	137.2	134.8	131.0	127.0
^{13}C β-pyrrole[b]	156.4	146.1	143.7	141.6	132.2	127.0
^{13}C β-pyrrole[b]	197.9	201.0	219.9	222.0	213.8	212.7
^{13}C methyl	-21.5	-17.0	-42.7	-42.4	-43.0	-42.9
^{13}C methyl	-38.2	-36.3	-38.8	-39.4	-39.6	-40.5
^{13}C methyl	-47.5	-49.3	-33.3	-32.2	-31.2	-30.1
^{13}C methyl	-56.7	-56.7	-32.1	-32.9	-31.9	-32.6
^{1}H methyl	13.21	10.89	23.95	23.66	23.33	22.83
^{1}H methyl	17.95	16.98	22.41	22.73	22.15	22.36
^{1}H methyl	24.88	25.47	22.46	21.63	20.76	19.67
^{1}H methyl	32.21	32.16	17.83	18.11	17.38	17.48

[a]Chemical shifts obtained from samples isotopically labeled with 5-^{13}C-ALA. [b]Chemical shifts obtained from samples isotopically labeled with 4-^{13}C-ALA.

Table S14. Individual Fe^{II} *Pa* WT shifts used as the δ_{dia} reference shifts.

^{13}C meso[a]	^{1}H meso[a]	^{13}C α-pyrrole[a]	^{13}C α-pyrrole[b]	^{13}C β-pyrrole[b]	^{13}C methyl	^{1}H methyl
98.3	9.33	146.3	146.3	144.0	15.2	3.35
99.7	9.45	147.5	146.6	144.4	13.1	3.46
99.9	9.48	147.5	149.2	145.3	15.4	3.51
100.8	9.93	149.1	149.3	145.5	15.0	3.73

[a]Chemical shifts obtained from samples isotopically labeled with 5-^{13}C-ALA. [b]Chemical shifts obtained from samples isotopically labeled with 4-^{13}C-ALA.

References

(1)   Zhong, L. H.; Wen, X.; Rabinowitz, T. M.; Russell, B. S.; Karan, E. F.; Bren, K. L.: Heme Axial Methionine Fluxionality in *Hydrogenobacter thermophilus* cytochrome *c*-552. *Proc. Natl. Acad. Sci. USA* **2004**, *101*, 8637-8642.

(2)   Can, M.; Zoppellaro, G.; Andersson, K. K.; Bren, K. L.: Modulation of Ligand-Field Parameters by Heme Ruffling in Cytochromes *c* Revealed by EPR Spectroscopy. *Inorg. Chem.* **2011**, *50*, 12018-12024.

(3)   Takayama, S. J.; Takahashi, Y.; Mikami, S.; Irie, K.; Kawano, S.; Yamamoto, Y.; Hemmi, H.; Kitahara, R.; Yokoyama, S.; Akasaka, K.: Local conformational transition of *Hydrogenobacter thermophilus* cytochrome *c*(552) relevant to its redox potential. *Biochemistry* **2007**, *46*, 9215-9224.